Hindawi
Adsorption Science & Technology
Volume 2023, Article ID 1911596, 19 pages
https://doi.org/10.1155/2023/1911596

Research Article

Characterization and Potential of *Samanea saman*-Activated Carbon on Adsorption of Copper from an Aqueous Solution

Achmad Chusnun Ni'am,[1] **Muhamad Suhar**,[1] **and Ernso Fenelon**[2]

[1]*Department of Environmental Engineering, Institut Teknologi Adhi Tama Surabaya, Arief Rachman Hakim Road No. 100, Surabaya 60117, Indonesia*
[2]*Centre de Recherche Interdisciplinaire pour la Vulgarisation Agricole et le Développement Local (CREIVADEL), Université NotreDame d'Haïti, Faculté d'Agronomie, BP HT 8110, Redon, Torbeck, Sud d'Haïti, Haiti*

Correspondence should be addressed to Ernso Fenelon; efenelon62@gmail.com

Received 24 December 2022; Revised 7 June 2023; Accepted 12 July 2023; Published 7 August 2023

Academic Editor: Senthil Kumar Ponnusamy

The mining and electroplating industries have resulted in the contamination of the environment with heavy metal. This has resulted in a serious threat to the ecological environment and human health due to the presence of copper pollution. To address this issue, extensive efforts have been made to develop effective methods for removing contaminants, particularly heavy metal, and *Samanea saman* (SS) was selected as precursor production of activated carbon. Therefore, this study is aimed at investigating *Samanea saman*-activated carbon (SSAC) to remove copper from an aqueous solution. SS was chemically activated by potassium carbonate and carbonized at 600°C for 5 hours, while SSAC was characterized by scanning electron microscopy-energy dispersive X-ray (SEM-EDS), Fourier-transform infrared (FTIR), and proximate tests. Copper adsorption on SSAC was evaluated by the Langmuir, Freundlich, Langmuir, Freundlich, Redlich-Peterson, Harkin-Jura, and Jovanovic models. Pseudo-first-order, pseudo-second-order, Elovich, and intraparticle diffusion models were used to identify adsorption process mechanism. SEM-EDS results presented that the pore of SSAC was heterogeneous, irregular in shape, and mesopore. In addition, FTIR analysis identified the main functional groups present in SSAC as C-H, C-O-C, and C-O. The proximate test conducted on SSAC determined the water content, volatile matter, ash content, and fixed carbon to be 0.61%, 22.26%, 9.77%, and 67.97%, respectively. The results showed that SSAC exhibited exceptional performance with copper removal efficiency of 99.49% under an adsorbent mass of 0.25 g, a reaction time of 30 minutes, and a concentration of 10 mg/L. Isotherm adsorption of SSAC followed the Redlich-Peterson model with an adsorption capacity (Qm) of 0.663 mg/g, correlation value (R^2) of 0.9992, and pseudo-second-order pattern $R^2 = 0.9997$. Therefore, SSAC can be proposed as a potential and economical biomaterial to treat heavy metal in wastewater.

1. Introduction

The surge in industrial growth over the past years can be attributed to a substantial increase in waste generation. Specifically, wastewater generated by various industries contains a range of metal. The mining, electroplating, and textile sectors are among the industries responsible for metal production, particularly copper (Cu). The recent increase in electronic products driven by the demand for advanced technology has led to a significant rise in the inclusion of metal, such as copper in their composition. Consequently, the scope of copper wastewater, containing Cu within industrial settings, is expanding accordingly. This metal can enter aquatic ecosystems through natural processes and human activities. It is released into the environment through erosion and weathering of rocks, and it can also be carried by rainwater from the atmosphere through natural means. On the other hand, human activities contribute to the contamination through the discharge of industrial wastewater. Even though metal is an essential mineral required in trace amounts for various metabolic processes in organisms, its high concentrations have toxic effects [1]. According to the

Agency for Toxic Substances and Disease Registry in 2019, copper is part of poisonous metal [2]. The poisoning can have an acute impact or accumulation in the body of an organism. Acute effects cause symptoms such as nausea, vomiting, abdominal pain, hemolysis, necrosis, and seizures and can result in death. The impact of this metal is chronic and can accumulate in the liver, causing hemolysis [3]. In Indonesia, there are numerous sources of organic and inorganic pollutants, but the metal processing and metallurgy sectors are mainly responsible for a substantial amount of contaminants posing serious risks to the environment and living beings. Furthermore, Indonesia is a leading producer of minerals, including copper (smelter and refinery). A rise in the number of metal industry has the potential to increase the amount of pollutants to produced. It is crucial to control copper levels in water through treatment before releasing it into the environment to mitigate the emerging negative effects.

Several treatment methods for reducing the concentration of copper in water have been reported, such as using composite hydrogel [4], ligand composite material [5], a mixture of algae waste-bentonite [6], natural zeolite [7], and hybrid fiber SiO_2-MgO [8]. Most of these techniques can be challenging to synthesize and expensive to produce, and the chemical compounds employed may generate waste as a by-product. In addition, the other various methods such as chemical precipitation, flocculation, membrane filtration, electrochemical treatment, and photocatalysis have similar challenges.

Alternatively, the utilization of adsorption method employing activated carbon can be considered, owing to its reliance on easily obtainable raw materials, straightforward manufacturing process, and cost-effectiveness. Adsorption exhibits numerous advantages over alternative approaches in the context of eliminating inorganic contaminants, including enhanced removal capacity even at lower concentrations [9]. Several studies have been conducted on producing activated carbon from natural materials, such as rice straw [10], coconut shells [11], betel nuts [12], and plant biomass [13]. Activated carbon emerges as a promising candidate for various adsorption applications. Conventional adsorbent materials can be modified to exhibit the characteristics, such as enhanced porosity and surface area. This can be achieved through physical methods, where the material is subjected to carbonization in the absence of oxygen [14]. Activated carbon can be produced from biomass materials sourced from cellulose, hemicellulose, lignocellulose, and lignin compounds [15].

Samanea saman (SS) is a shade plant often found on the road and belongs to the *Fabaceae* family scattered in the tropics [16]. Previous results indicated that carbon content is relatively high, making it a viable option as activated carbon material. Several studies analyzed the elemental composition of the seed fruit before treatment, showing significant carbon of 56.41%, with nitrogen, hydrogen, and oxygen at 1.42%, 8.10%, and 33.11%, respectively. Another study explored the production from *Cassia fistula* (golden shower), which belongs to the same family as SS, namely, *Fabaceae*. Consequently, it can be inferred that SS possesses substantial potential as a raw material for the production of activated carbon [17]. However, there was no inquiry into the potential and characterization of activated carbon used to remove copper in an aqueous solution. This study observed adsorption effectivity of copper using biomass plants rarely developed from the *Fabaceae* family. SS was one of the new alternative potentials used in heavy metal [13]. *Samanea saman*-activated carbon (SSAC) was synthesized and demonstrated for adsorption in copper aqueous. SSAC synthesis was carried out using a high-temperature furnace with a K_2CO_3 activator. K_2CO_3 was selected because it was more environmentally friendly than acid or base activators. Activated carbon characterization tests included surface pore conditions, active groups, iodine number, and proximate analysis. The batch study explored adsorption process under various conditions, such as initial concentration, pH, adsorbent mass, and time. The study adsorption isotherm model was the Langmuir and Freundlich isotherm representing a model of adsorption with a monolayer [18]. Adsorption isotherm served as a valuable tool for understanding the dynamics of adsorption process and evaluating the efficacy of the adsorbent in interacting with adsorbate [19], and Langmuir and Freundlich isotherms were often used [20]. Adsorption kinetics studies were carried out to determine the equilibrium of adsorption process using pseudo-first-order and pseudo-second-order models [21]. Based on the description, SSAC has been investigated for the removal of copper. The effect of operational parameters such as copper concentration, pH, mass adsorbent, time, and adsorption isotherm was also examined to describe adsorption mechanism of copper using SSAC. The limitation scope of this study was desorption study of tested pollutants, as well as the binary and ternary adsorption processes.

2. Material and Methods

2.1. Materials. Sodium hydroxide (NaOH), hydrochloric acid (HCI), and potassium carbonate (K_2CO_3) were purchased from Loba Chemie grade proanalysis. The solutions were prepared from the ultrapure water system. The pH meter from the ADWA AD1200 was used to measure the pH of solutions. Copper stock solution of 1000 mg/L in ultrapure water was prepared using copper standard solution ($Cu(NO_3)_2$ and was purchased from Merck.

2.2. Activated Carbon Preparation. The preparation of activated carbon follows numerous steps. The *Samanea saman* plant was discovered, and its fruit was collected on a Gresik City sideroad. The fruit peel characterization is black color and reasonably straight. Fruit peels were washed several times and dried in the shade away from impurities. Furthermore, the fruit peel was dried in an oven at 80°C within 24 hours. Fruit peel was grounded and sieved to obtain a particle size of 0.25 mm [13, 22]. *S. saman* peels were activated through a chemical process with K_2CO_3 at a mass ratio of 3 : 1. *S. saman* peels were pyrolyzed at 600°C for 5 hours. After pyrolysis, activated carbon was rinsed with HCl 0.1 N and washed with demineralized water until pH neutral. The activated carbon stock was stored in a closed dry dark bottle at room temperature standard with a humidity of 45%-65% [22].

2.3. Batch Adsorption Experiments. In this study, the adsorption process used a batch system. The experiment occurred in duplicate with various variables such as pH (4, 7, and 9), concentration (10 mg/L, 20 mg/L, 30 mg/L, and 40 mg/L), and activated carbon mass (0.01 g, 0.25 g, 0.5 g, 0.75 g, and 1.0 g). The samples were stirred for 90 minutes at a speed of 180 rpm. The filtrate was analyzed to determine copper concentrations contained in the aqueous solution that had been adsorbed. The concentration value test will be carried out using a spectrophotometric tool using the APHA method, Method 3111 B: 2017. Equilibrium copper concentrations were determined using an atomic absorption spectrophotometer, the Perkin Elmer AAnalyst 300 with an air-acetylene flame. The adsorption efficiency (%) of copper was calculated by the equation.

$$A(\%) = \frac{\mathrm{Co} - \mathrm{Ce}}{\mathrm{Co}} \times 100\%. \quad (1)$$

The symbols used in the equations for adsorption removal percentage are initial and final concentrations (in mg/L) represented by Co and Ce, respectively.

2.4. Activated Carbon Characterizations. This study determined the physicochemical characteristics of SSAC. Proximate analysis was carried out according to the ASTM D7582-10. The results are presented in terms of water content, volatile content, fixed carbon, and ash contents. In this study, the adsorption capacity of activated carbon was analyzed using the iodine number. Iodine adsorption used the sodium thiosulfate volumetric method.

The iodine number can reasonably approximate active carbons' surface area and microporosity [23].

The surface morphology of the adsorbent investigated was analyzed using scanning electron microscopy (Hitachi FlexSEM 1000). It also provides information about the structure, i.e., the porous adsorbent. The surface functional groups of SSAC were analyzed using Fourier-transform infrared (FT-IR) spectroscopy (Perkin Elmer Spectrum Two).

2.5. Statistical Analysis. All experiments were carried out in duplicate. The adsorption equilibrium model could be determined based on the linear coefficient of determination (R^2) value and supported by the statistical test of nonlinear Chi-square (χ^2). The value of R^2 is obtained on the graph of the adsorption isotherm equation, and the adsorption order rate equation then determines the highest near 1.

$$\chi^2 = \sum \frac{\left(q_{e,\mathrm{exp}} - q_{e,\mathrm{cal}}\right)^2}{q_{e,\mathrm{cal}}}, \quad (2)$$

where $q_{e,\mathrm{exp}}$ (mg/g) is the adsorption capacity at equilibrium and $q_{e,\mathrm{cal}}$ (mg/g) the adsorption capacity determined from the adsorption model.

3. Results and Discussion

3.1. SSAC Proximate and Iod Number Analysis. The proximate analysis of *S. saman*-activated carbon (SSAC) and commercial-activated carbon (CAC) is presented in Table 1.

Moisture content refers to the quantity of water present in a material. The analysis of water content in SSAC-activated carbon and CAC yielded a value of 0.61% and 1.73%, respectively. It is worth noting that high water content can have an impact on the hygroscopic characteristics of activated carbon. In contrast, a lower moisture content indicates a reduced amount of residual water covering carbon pores [24].

Ash content refers to the residual minerals that evaporate during the carbonization process. The analysis showed that SSAC and CAC had an ash content of 9.77% and 9.94%, respectively. Ash content plays a significant role in determining the quality of activated carbon, and a high amount can lead to the closure of pores, resulting in a reduced carbon surface area [25].

The analysis purpose of volatile substance levels is to determine the content of compounds that can evaporate at heating to 950°C. At heating above 900°C, elements such as nitrogen and sulfur can evaporate due to their volatile nature. The analysis showed that SSAC-activated carbon and CAC had volatile substance levels of 22.26% and 27.56%, respectively. Elevated levels of these substances indicated the presence of noncarbon compounds attached to carbon surface, particularly hydrogen (H) and oxygen (O) elements. These elements were bound firmly to the carbon surface in the form of CO_2, CO, CH_4, and H_2 [26].

Fixed carbon is the amount of pure carbon contained in a sample used to determine the value of material. Meanwhile, bound carbon is calculated based on the value of volatile substances and ash content. The calculation results reported SSAC-activated carbon and CAC of 67.97% and 62.50%, respectively [24].

The iodine number is the defined amount of iodine absorbed by 1 gram of adsorbent. It can be used to estimate the area of exposure and porosity of activated carbon. From analytical results, the iodine number from each SSAC and CAC-activated carbon were 996.8 mg/g and 760.4 mg/g, respectively. The iodine number of SSAC was higher than commercial CAC; hence, it had a better porosity [23, 27].

3.2. Morphological and Functional Analysis. Morphological characterization was performed using SEM-EDS. SEM can analyze the surface of a material structure and provide microstructure information of a material, including morphology, texture, and crystallography. The instruments are also supported by EDS analysis (Figure 1) to obtain the microphysical condition of material structure and related information from the element in a material [28].

The surface morphology result is shown in Figure 1. SEM results presented that the surface morphology of SSAC was heterogeneous and irregular with sponge-like pores. The structure of a porous surface, such as a sponge, was expected to increase the outer surface of the adsorbent to increase adsorption capacity. These pore structures were obtained

Table 1: Proximate analysis of *S. saman*-activated carbon and commercial-activated carbon.

No.	Proximate analysis (wt%)	SSAC	CAC
1	Moisture	0.61	1.73
2	Ash	9.77	9.94
3	Volatile	22.26	27.56
4	Fixed carbon	67.97	62.50

due to the evaporation of activator K_2CO_3 during the pyrolysis process.

The surface condition of SSAC before adsorption (Figure 1(a)) was discernible, with numerous unfilled pores visible. However, in SSAC after adsorption (Figure 1(b)), there was a noticeable increase in the number of particles adsorbed onto the surface and within the pores. Additionally, the spectrum analysis presented the presence of a copper metal signal on the SSAC sample after adsorption.

FTIR analysis was used to determine active functional groups in a material. This functional group played a vital role in the adsorption of activated carbon cystitis. The functional group also affected the adsorption activity of the adsorbent. The samples carried out by FTIR analysis were SS material before activation and adsorption, as well as after adsorption. FTIR analysis results are shown in Figure 2.

FTIR analysis on SS powder denoted a vibrational (O-H) hydroxyl bond at wave absorption of 3277.60 cm^{-1}. The aromatic C=C bond stretch was established at a wave absorption of 1404.94 cm^{-1} and strengthened by C-H bond stretch vibration at 2921.81 cm^{-1} [29]. The infrared spectrum of *SS* powder also denoted the presence of a stretch carboxylic bond (C=O) at wave absorption of 1614.36 cm^{-1}, and the C=O group was a characteristic of a flavonoid compound [30]. The C-O group and C-O-SO_3 bond were at a wave absorption of 1032.76 cm^{-1} and 865.05 cm^{-1}, respectively. The bond of CH_2 aliphatic alkane was demonstrated at a wave absorption of 776.52 cm^{-1} [21]. From the analysis results, the infrared spectrum of SS contained active functional groups O-H, C=C, C-H, C=O, C-O, C-O-SO_3, and CH_2.

The functional group shown on SSAC was a C-H bond at a wave absorption of 2973.22 cm^{-1}. The infrared spectrum at wave absorption of 1054.87 cm^{-1} has a sharp peak, typical for C-O-C bonds on cellulose or polysaccharides [21]. Furthermore, the C-O cluster was also identified at a wave uptake of 1033.26 cm^{-1}. From the infrared spectrum analysis, SSAC had active functional groups C-H, C-O-C, and C-O.

Samples of FTIR analysis for SSAC after adsorption presented C-H bonds at an adsorption wave of 2973 cm^{-1}. The sharp spectrum at wave number 1054.87 cm^{-1} showed the vibration of the C-O-C bond. At wave number 1033.26 cm^{-1}, a sharp peak indicated the vibration of the C-O bond. Therefore, the functional groups obtained from the IR spectrum analysis on SSAC after adsorption were C-H, C-O-C, and C-O. The spectrum comparison of the three samples can be listed in Table 2.

From Table 2, it was found that the functional group changed between SS powder and SSAC. This happened because several functional groups, such as O-H, C=O, and C-OH, evaporated into CO_2, CO, and H_2O during carbonization process. The mechanism of carbonization reaction can be illustrated in Figure 3.

Functional groups on SSAC before and after impregnation showed almost the same IR spectrum pattern. However, the peak transmission intensity of SSAC after impregnation was smaller than SSAC after conducting further analysis. This decrease or change was due to the presence of analyte adsorption activity by activated groups on the surface of activated carbon [21]. The presence of this activity caused the free active group to decrease, decreasing the transmission value. The adsorption mechanism of Cu^{2+} ions on the active groups of activated carbon is illustrated in Figure 4.

3.3. Effect of Concentration. An aqueous concentration is one of the most critical factors during adsorption. The effect of initial concentration on copper adsorption was studied for 90 minutes at each initial concentration (10-40 mg/L). The copper solution was placed in contact with a mass of activated carbon 0.5 g and stirred at 180 rpm. According to Figure 5, SSAC depicted the optimum adsorption concentration at 10 mg/L with an average removal of 98.32%. Adsorption ability was decreased with an average removal of 73.94%, 53.4%, and 46.93% in the concentration of 20 mg/L, 30 mg/L, and 40 mg/L, respectively. In line with SSAC, CAC indicated the optimum adsorption concentration at 10 mg/L with an average removal of 61.91%. Adsorption ability was decreased with an average removal of 39.30%, 28.27%, and 27.3% in the concentrations of 20 mg/L, 30 mg/L, and 40 mg/L, respectively.

The large structure of internal pores consisting of macropores, mesopores, and micropores influences an adsorbent's adsorption authority. Furthermore, the pore volume and size distribution on the surface of activated carbon were related to adsorption capacity [13]. Figure 5 indicated that SSAC had a higher adsorption ability than CAC in all concentrations. The results of testing also supported that the iodine number of SSAC was more remarkable than CAC.

The adsorption capacity of activated carbon demonstrated a decrease corresponding to the rising copper concentration. This decline was attributed to the saturation of the surface, and when the adsorbent reached the saturation point, the concentration remained unchanged or decreased [31]. Activated carbon adsorption process dissolved on a heterogeneous monolayer surface [32]. In the monolayer adsorption process, adsorption probability on the surface layer decreased when activated carbon surface was saturated or completely covered. In this condition, the absorption capacity of the adsorbent had reached its maximum limit, and the removal process decreased as the analyte concentration increased.

3.4. Effect of pH. One of the crucial factors affecting the interaction of substances is pH. The effect of pH is carried out in various pH conditions (4, 7, and 9) at a stirrer speed of 180 rpm for 90 minutes. The analytical results of the percent removal of copper are presented in Figure 6. It can be seen from the figure that the percentage removal slightly increases with the increase in pH. Copper adsorption using

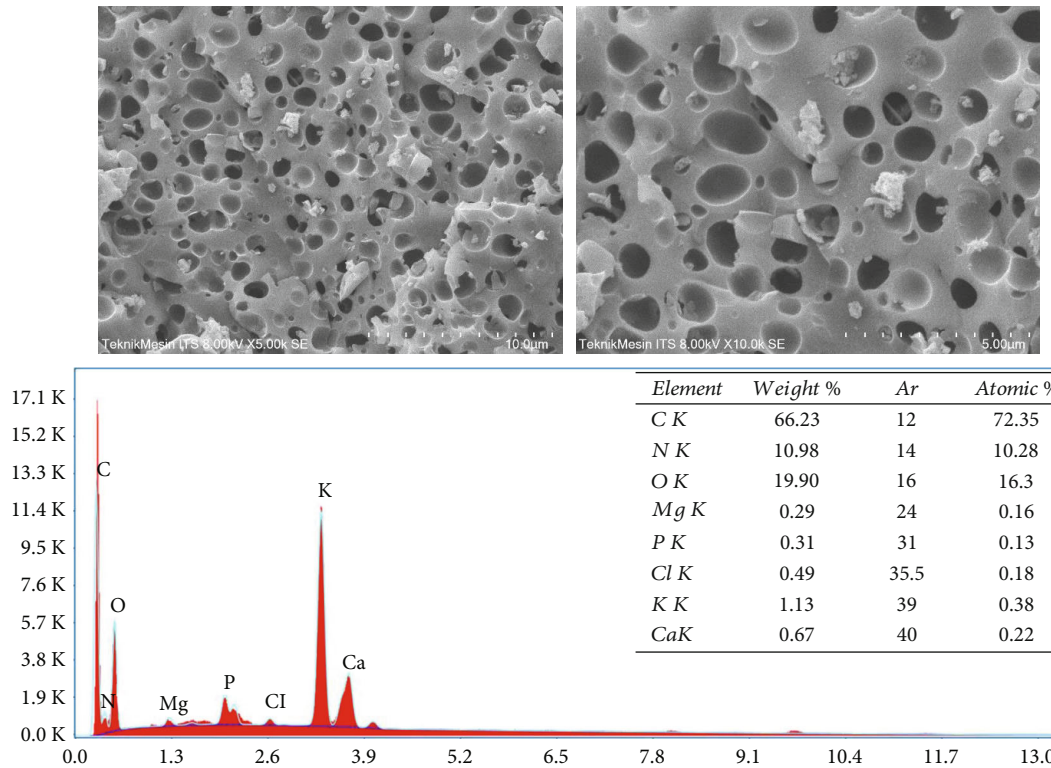

Element	Weight %	Ar	Atomic %
C K	66.23	12	72.35
N K	10.98	14	10.28
O K	19.90	16	16.3
Mg K	0.29	24	0.16
P K	0.31	31	0.13
Cl K	0.49	35.5	0.18
K K	1.13	39	0.38
CaK	0.67	40	0.22

(a)

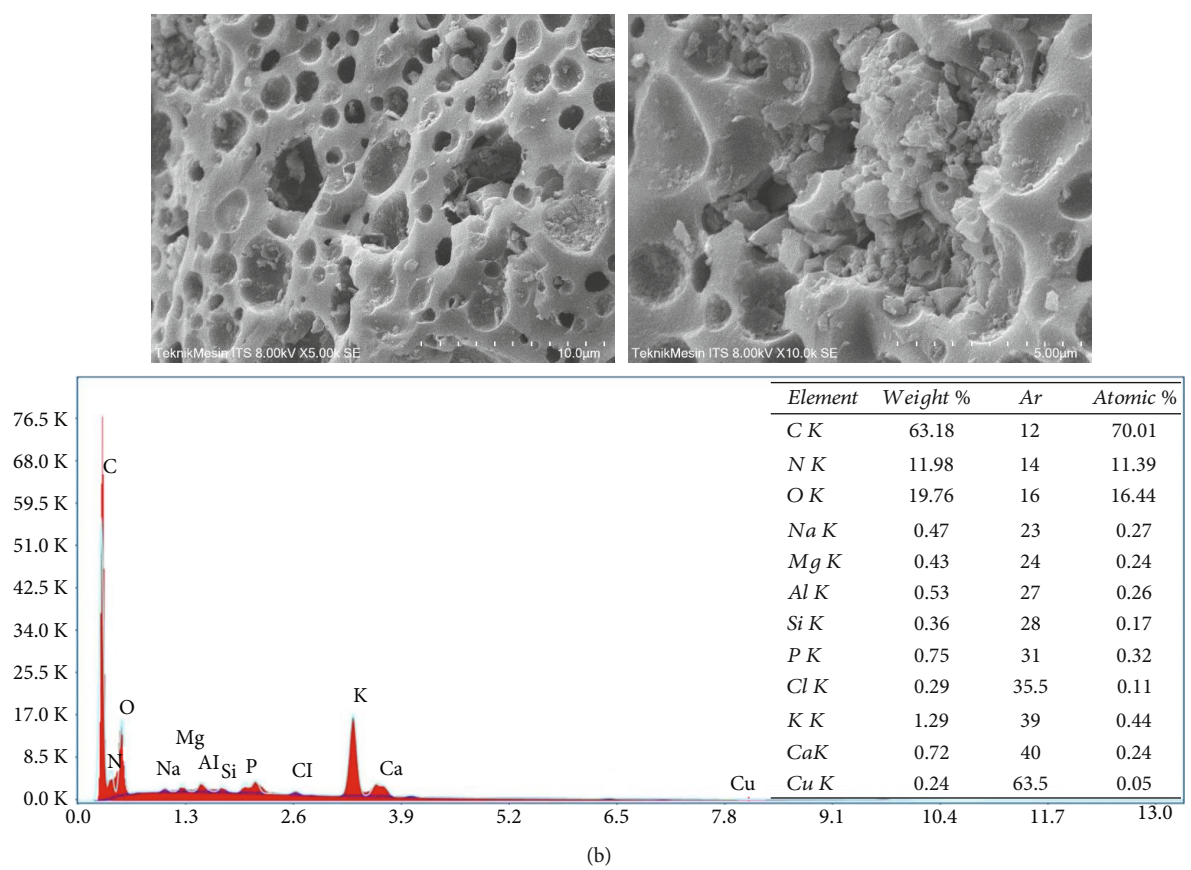

Element	Weight %	Ar	Atomic %
C K	63.18	12	70.01
N K	11.98	14	11.39
O K	19.76	16	16.44
Na K	0.47	23	0.27
Mg K	0.43	24	0.24
Al K	0.53	27	0.26
Si K	0.36	28	0.17
P K	0.75	31	0.32
Cl K	0.29	35.5	0.11
K K	1.29	39	0.44
CaK	0.72	40	0.24
Cu K	0.24	63.5	0.05

(b)

Figure 1: SEM-EDS result of SSAC activation (a) before adsorption and (b) after adsorption.

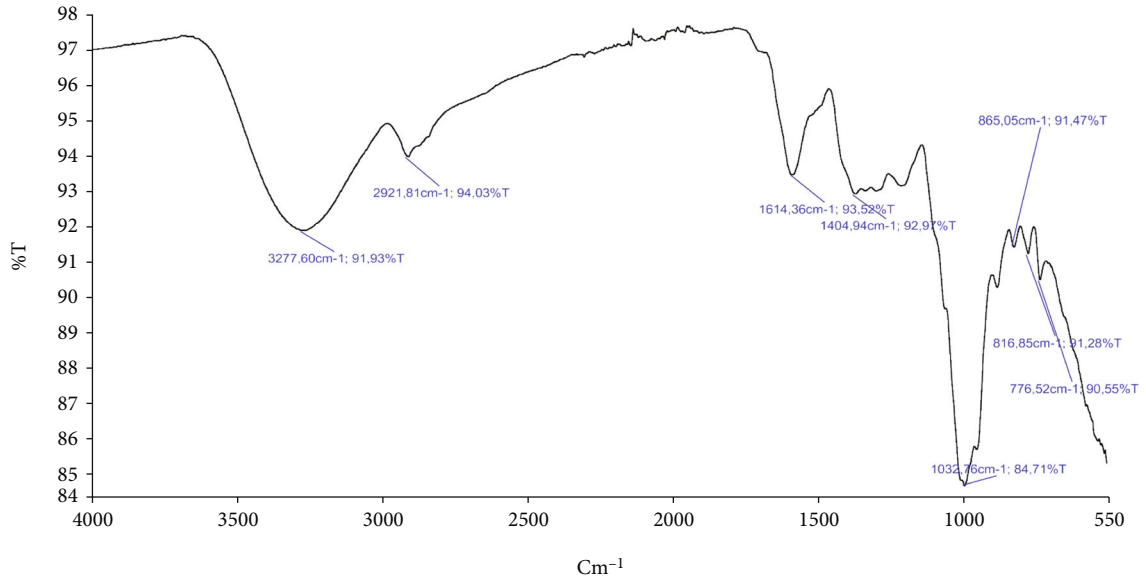

(a)

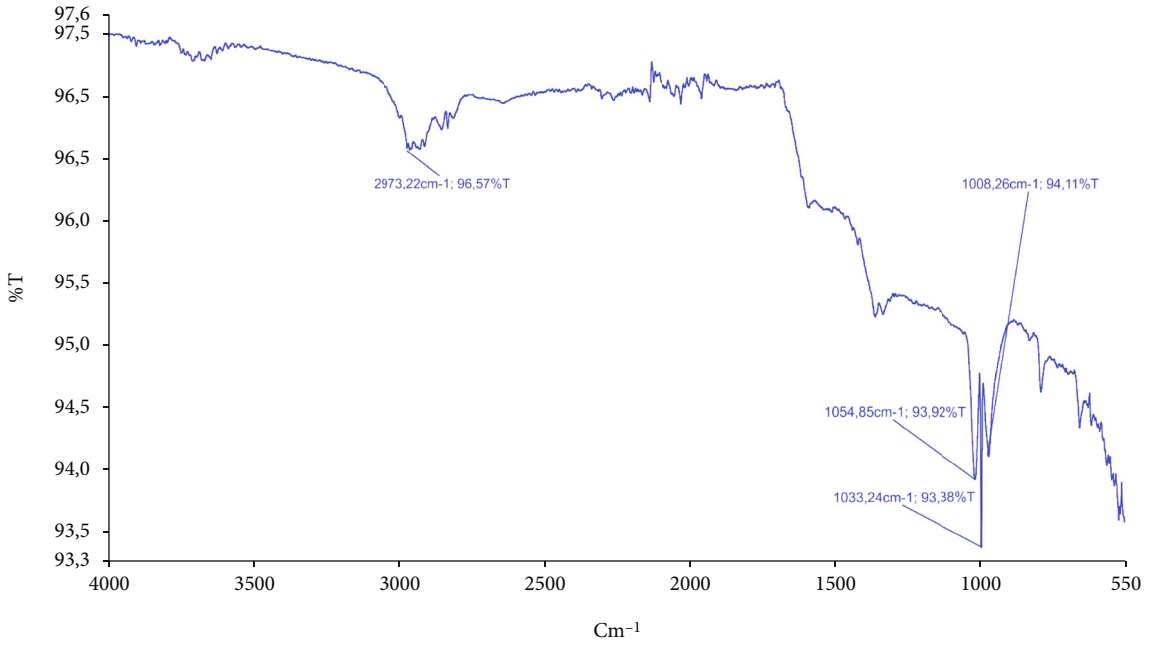

(b)

Figure 2: Continued.

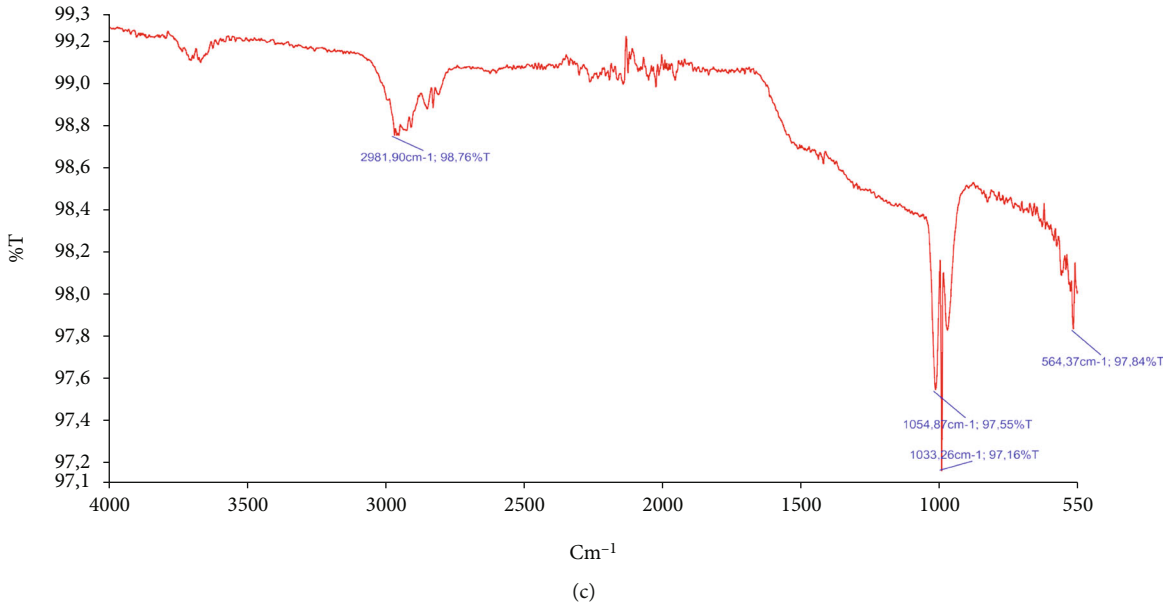

Figure 2: FTIR spectra of (a) *Samanea saman* powder, (b) SSAC before adsorption, and (c) SSAC after adsorption.

Table 2: Chemical bonding in *Samanea saman* material.

Bond	Peak wave absorption (cm^{-1})					
	SS powder		SSAC		SSAC impregnated	
	λ (cm^{-1})	A^*	λ (cm^{-1})	A^*	λ (cm^{-1})	A^*
O-H	3277.60	0.0807	—	—	—	—
C-H	2921.81	0.0597	2973.22	0.0343	2973.0	0.032
C=O	1614.36	0.0648	—	—	—	—
C=C	1404.94	0.0273	—	—	—	—
C-O-C	—	—	1054.85	0.0608	1054.87	0.0255
C-O	1032.76	0.1529	1033.24	0.0620	1033.26	0.0240
C-O-SO_3	865.05	0.0853	—	—	—	—
C-H_2	776.52	0.0945	—	—	—	—

*Adsorption ($A = 1 - T\%$).

SSAC is higher than CAC. The percentage of copper removal with SSAC at pH 4, 7, and 9 tends to increase at 98.75%, 98.75%, and 99.81%, respectively. The percentage of copper removal in CAC has increased along with an increase of pH in 84.44%, 85.85%, and 90.87%, respectively.

The pH has dual effects on metal sorption, influencing the solubility and speciation of metal ions in solution, as well as the overall charge of the sorbent. The acidity level can alter the resonance of bonds (single or double) in the active groups present on the surface of activated carbon. Consequently, variations in pH can impact the reaction kinetics and the equilibrium point during adsorption process. In an acidic environment, the active groups on the adsorbent surface are subjected to protonation in response to the presence of H+ ions [33]. In an acidic atmosphere, the process of adsorption of metal can occur because this metal dissolves as cations to be well adsorbed. However, when the charge and the protonation adsorbent surface are positively charged, there will be a repulsive reaction competition between the H^+ ion and positively charged metal ions [34].

In alkaline conditions, OH^- ions deprotonate the active group on the adsorbent surface and form negative ions. Positively charged metal ions are attracted to the adsorbent surface to increase the adsorption process. However, metal in an alkaline atmosphere experience a decrease in water and precipitate as a hydroxide. A decreased copper metal concentration in an alkaline atmosphere can occur due to adsorber or precipitating in $Cu(OH)_2$[33]. The Distribution of Cu(II) species as a function of pH is illustrated in Figure 7.

Under neutral conditions, H^+ and OH^- ions are at an equilibrium point. Therefore, the competition of H^+ ions and deposition of metal due to reacting with OH^- are relatively small. Positively charged metal ions can interact on the surface of adsorbents containing carbon atoms binding to oxygen. Furthermore, oxygen elements with two pairs of free electrons are more likely to be negatively charged to interact with positively charged elements.

The degree of acidity significantly affects functional (active) groups such as C=OOH, -CHO, and -OH. The

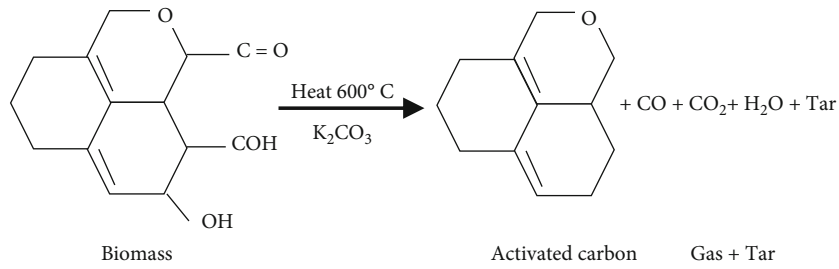

Figure 3: Illustration of the activated carbon synthesis mechanism (author's original image illustration).

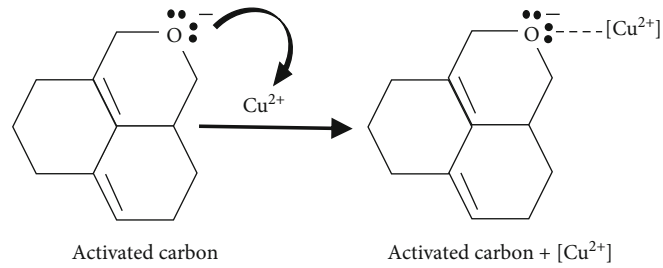

Figure 4: Illustration of Cu^{2+} ion adsorption mechanism (author's original image illustration).

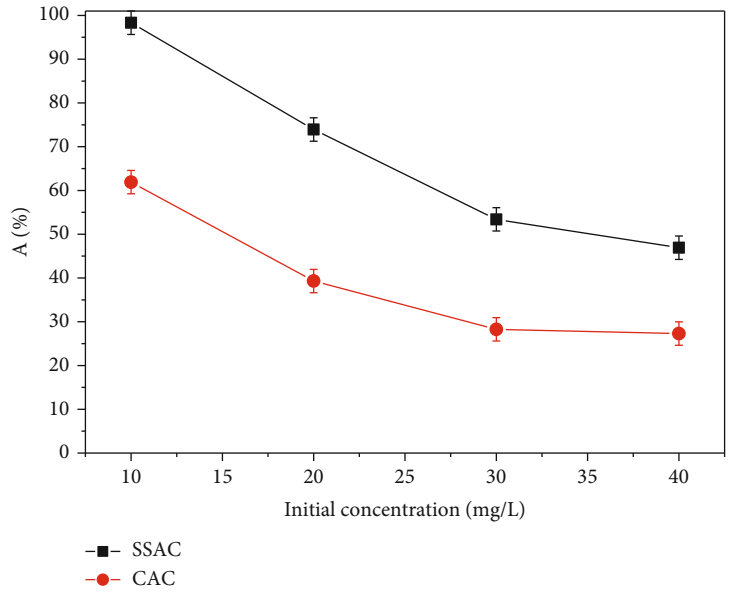

Figure 5: Effect of initial concentration on the adsorption of copper onto SSAC and CAC (adsorbent mass = 0.5 g; pH = 4, agitation speed = 180 rpm; time = 90 minutes).

mechanism of ion change on the side of the active group under acidic, basic, and neutral conditions can be illustrated in Figure 8. In addition to the active functional groups on the adsorbent surface, pH affects the solubility of metal in water. $Cu(OH)_2$ precipitates begin to form when the pH rises above 7. Therefore, in the adsorption process under alkaline conditions, it is difficult to determine whether metal concentration is reduced due to adsorption or the deposition process. Following the results, the optimum working conditions for the Cu adsorption process are at range of pH 2–6 [35].

3.5. Determination pH Point Zero Charge. The pH at the point of zero charge (pH_{ZPC}) represents a state where the surface of a material is electrically neutral. The pHpzc is determined by the point of intersection between the initial and final pH curves [36]. The pH_{ZPC} value of SSAC and CAC- activated carbon is shown in Figure 9.

Figure 9 shows that the pH_{ZPC} for SSAC and CAC are 7.56 and 7.35, values greater than the optimum pH. This ZPC value indicates that SSAC and CAC adsorbents tend to have a positive charge. Adsorbents possessing a positive

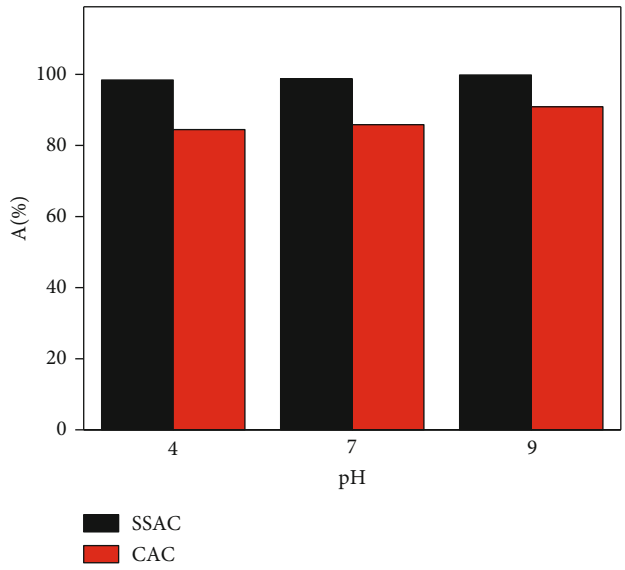

Figure 6: Effect of pH on percentage removal of copper by SSAC and CAC (initial concentration 10 mg/L; adsorbent mass 0.5 g; agitation speed 180 rpm; time 90 minutes).

charge guarantee their adeptness in adsorbing the adsorbate below the pH of optimal adsorption [37].

3.6. Effect of Adsorbent Mass. The effect of adsorbent mass on copper adsorption ability is shown in Figure 10. The copper adsorption using SSAC is higher than CAC. The adsorption ability of SSAC has increased in an amount of 0.05 g, 0.10 g, and 0.25 g with a removal percentage of 90.45%, 97.46%, and 99.49%, respectively. Meanwhile, the removal is relatively stable at the mass of 0.5 g, namely 99.45%, and has decreased slightly at 0.75 g and 1 g with 99.23% and 99.25%, respectively. The adsorption ability of CAC increased at levels of 0.05 g, 0.10 g, and 0.25 g with a removal of 74.44%, 80.84%, and 85.49%, respectively. At levels of 0.5 g, 0.75 g, and 1 g, the removal decreased by 85.13%, 84.13%, and 84.99%, respectively.

The effect of mass on the removal of copper shows a tendency to decrease the level of adsorption as the number of mass administered increases. An excessive quantity of adsorbent mass results in the overlapping of certain active areas within the adsorbent. This overlapping effect hinders the effective dispersion and maximal adsorption of metal ions by a particular active area of the adsorbent [13, 38]. Adding higher mass to the adsorbent can cause aggregations that reduce the area of the active site of the adsorbent, resulting in a decrease in adsorption capacity [13, 39].

3.7. The Effect of Time. The suitability of adsorption equilibration is affected by contact time. The effect of contact time on the adsorption efficiency of copper onto SSAC and CAC increased from 0.5 to 30 min, as presented in Figure 11. Copper adsorption was insignificant after 15 minutes, and the process reaches the equilibrium at 15 min for both SSAC and CAC. As shown in Figure 11, the adsorption of SSAC reaches equilibrium faster than CAC.

The adsorption ability of each activated carbon is significantly improved at the beginning time. Therefore, there are many pores and activated areas on carbon surface that have yet to be filled by adsorbates. In a longer contact time, the capacity runs more constantly due to the increase in adsorbate saturation of the active area of the adsorbent [40]. From the time of optimization treatment, the adsorption process occurs in the fast and slow stages. The fast or initial stage is where adsorption process increases significantly, while the slow stage is when the adsorbent and adsorbate are at equilibrium. At this stage, the adsorption power of the adsorbent against the adsorbate has reached the saturation point [40].

3.8. Adsorption Isotherms. The analysis of adsorption isotherms is fundamental to describing activated carbon performance in the solute process of some adsorbent masses. The purpose is to explain how adsorbent interacts with adsorbate and describe the magnitude of adsorption capacity. The study is modeled on Langmuir, Freundlich, Redlich-Peterson, Harkin-Jura, and Jovanovic Iiotherm [41]. Langmuir isotherms define the maximum capacity an adsorbent can occur due to a single layer of adsorbate above the adsorbent surface. The calculation of this isotherm is conducted according to the equation below [42].

$$\frac{\text{Ce}}{\text{Qe}} = \frac{1}{\text{Qm}}.\text{Ce} + \frac{1}{K_L.Qm}, \tag{3}$$

where Ce is copper concentration at equilibrium (mg/L), Qe is adsorption capacity of copper at equilibrium (mg/g), K_L is the equilibrium constant of Langmuir adsorption isotherm, and Qm is the saturated adsorption capacity (mg/g).

The isotherm graph has 1/Qe on the y-axis and 1/Ce on the x-axis; hence, the linear line equation ($y = bx + a$) determines Qm and K_L values; Qm value is $1/a$, while K_L is the $1/b$. Qm value. From the equation, Langmuir can explain the type of its isotherm by calculating the separation factor (R_L), with the following equation [39].

$$R_L = \frac{1}{1 + K_L C_o}. \tag{4}$$

There is an optimum copper concentration where K_L is the Langmuir constant and Co. The adsorption can occur linearly or irreversibly when $R_L = 1$ or $R_L = 0$. The adsorption is either unfavorable or favorable when $R_L > 1$ or $0 < R_L < 1$, respectively [41].

Freundlich's decree describes the bond between adsorbate and adsorbent obtained from testing or laboratory study. To obtain the values of the provisions K_f and 1/n, it is necessary to create a linear line for the following equation [42].

$$\text{Log}(\text{Qe}) = \text{Log}K_f + \frac{1}{n}\text{LogCe}. \tag{5}$$

The Freundlich isotherm model can also explain whether adsorption is favorable, unprofitable, or irreversible using n. Generally, when $2 < n < 10$, $1 < n < 2$, and $n < 1$,

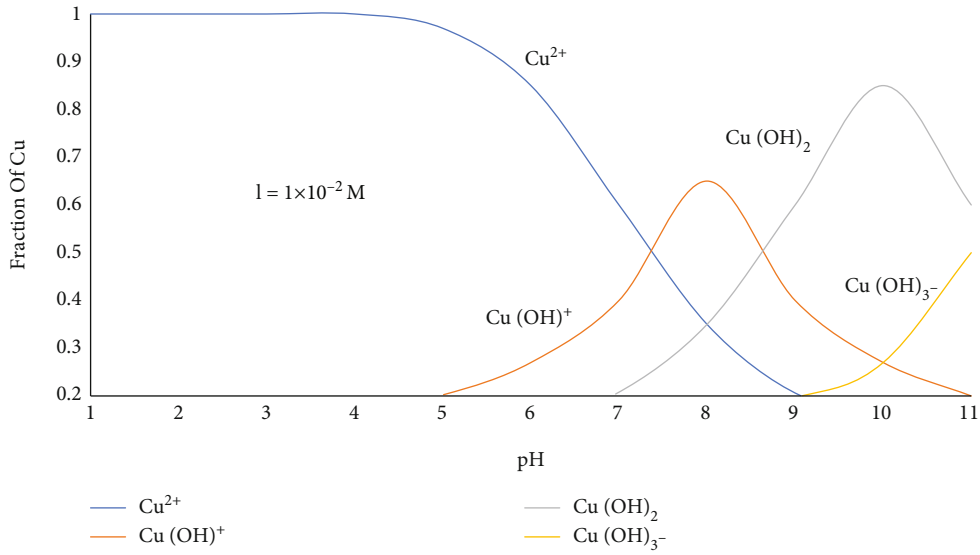

Figure 7: Distribution of Cu(II) species as a function of pH (redrawing from [35]).

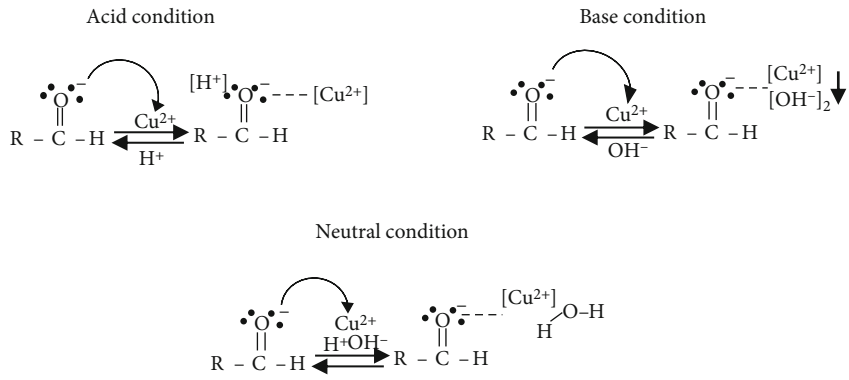

Figure 8: Activated group protonation mechanism at different pH (author's original image illustration).

the sorption characteristics are good, moderately difficult, and poor [21, 43].

The Redlich-Peterson isotherm is a mix of Langmuir and Freundlich. The numerator is from the Langmuir isotherm and has the benefit of approaching the Henry region at infinite dilution [44, 45]. This model is an empirical isotherm incorporating three parameters and combining elements from both the Langmuir and Freundlich equations. Therefore, the mechanism of adsorption is a mix and does not follow ideal monolayer adsorption [44, 45]. The linear equation of the Redlich-Peterson isotherm model:

$$\mathrm{Ln}\frac{\mathrm{Ce}}{\mathrm{Qe}} = \beta \mathrm{LnCe} - LnA. \tag{6}$$

The value of the Redlich-Peterson constant (β) is obtained by making a linear curve Ln Ce/Qe as the Y-axis and Ln Ce as the X-axis. The slope value of the linear equation is the Redlich-Peterson constant (β) [37].

The Harkin-Jura isotherm describes the process taking place on the surface of an adsorbent as multilayer adsorption. This phenomenon occurs due to the presence of a heterogeneous pore distribution within the adsorbent [44, 46]. Figure 12(b) illustrates the multilayer adsorption process. The linear equation of the Harkin-Jura isotherm model can be expressed as follows:

$$\frac{1}{\mathrm{Qe}^2} = -\frac{1}{A}\mathrm{Log\,Ce} + \frac{B}{A}. \tag{7}$$

A and B are the Harkin-Jura constants, which possess specific values depending on the adsorbent and adsorbate systems under consideration. The calculation of the constant value is obtained from the value of the graph slope $1/\mathrm{Qe}^2$ versus Log Ce.

The Jovanovic model has the same assumptions as the Langmuir which proposes monolayer adsorption on a homogeneous solid surface. However, the model also considers the possibility of mechanical contact between adsorbed and desorbed molecules. The linear equation of the Jovanovic isotherm model can be expressed as follows:

$$\mathrm{Ln}\,Q_e = -K_f \mathrm{C_e} + Ln\,Q_{\max}. \tag{8}$$

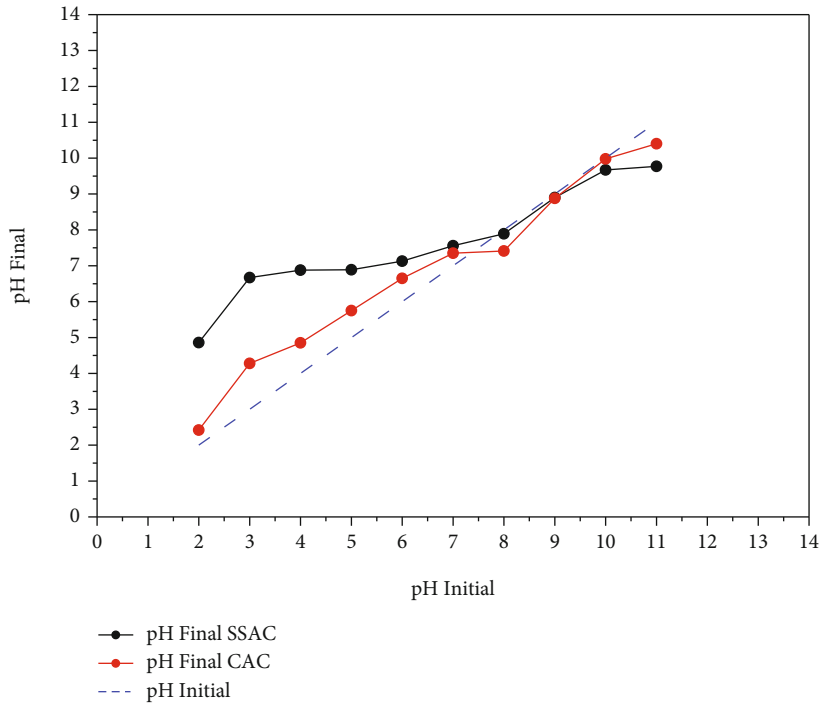

Figure 9: PZC for SSAC and CAC.

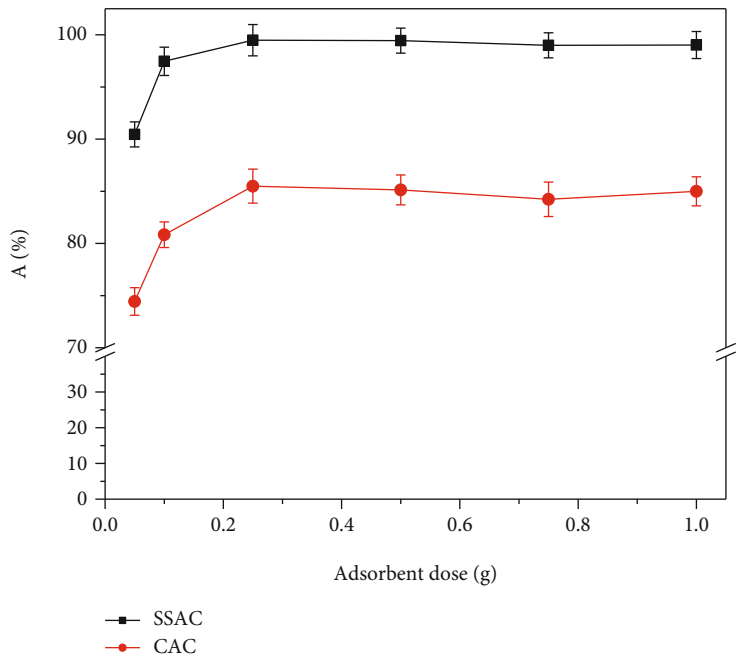

Figure 10: Effect of adsorbent mass on the adsorption of copper onto SSAC and CAC (initial concentration 10 mg/L; pH = 7, agitation speed = 180 rpm; time = 90 minutes).

The K_f value is a Jovanovic isotherm constant, obtained from the slope value of the linear regression curve Ln Q_e versus Ce.

The best adsorption isotherm model is determined by analyzing the coefficient of determination (R^2) because this analysis can measure the distribution of adsorbate, analyze the adsorption system, and verify the consistency of the model. The grouping results of Cu^{2+} ion adsorption isotherm modeling using SSAC and CAC are shown in Figure 13, and the calculated data are presented in Table 3.

Based on the five models performed, the best coefficient of determination (R^2) for Cu^{2+} ion adsorption is 0.9992

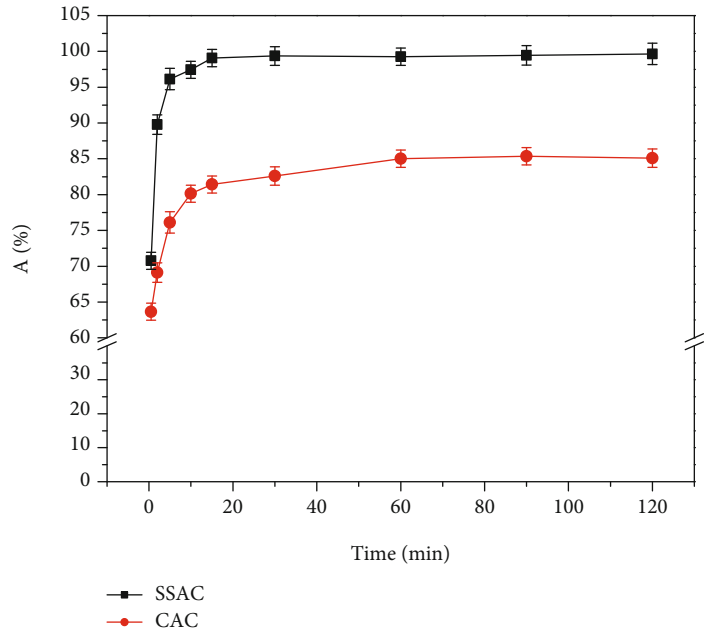

Figure 11: Effect of time on the adsorption of copper onto SSAC and CAC (initial concentration 10 mg/L; pH = 7, agitation speed = 180 rpm; adsorbent mass = 0.25 g).

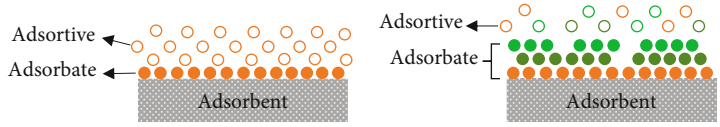

(a) Monolayer adsorption (a) Multilayer adsorption

Figure 12: Adsorption mechanism (author's original image illustration).

SSAC and 0.9815 CAC. SSAC and CAC-activated carbon have the best model fit on the Redlich-Peterson adsorption isotherm. Furthermore, the Redlich-Peterson is a composite adsorption isotherm model that combines Langmuir, Freundlich, and Henry. This model offers a broader range of applicability in representing adsorption equilibrium across various concentrations. The adsorption mechanism observed using the Redlich-Peterson model is a mixture, deviating from the ideal monolayer adsorption mechanism [44].

In the Redlich-Peterson equation, there are parameters A and B as a constant and indexes of heterogeneity, with a value range of 0-1. In addition, when the value of $\beta = 1$ or close to 1, $\beta > 1$ or far exceeds 1, and $\beta = 0$, the isotherm is simplified to the Langmuir, Freundlich, and Henry isotherm [44]. Based on the calculation data presented in Table 3, the Redlich-Peterson (A) constant values for SSAC and CAC are determined as 2.0534 L/g and 5.7495 L/g, while the values of β are 0.8761 and 0.7533, which are close to 1. This indicates that the isotherm model can be simplified to the Langmuir Isotherm, implying a non-ideal monolayer adsorption process. The simplified model can be applied to homogeneous and heterogeneous systems due to its versatility. Figure 12(a) illustrates the monolayer adsorption process. According to the model, the adsorption capacity (Q_m) can be determined based on the Langmuir isotherm. The calculated values for Q_m are 0.663 mg/g and 0.409 mg/g for SSAC and CAC, respectively.

The calculation of the Chi-Square and error function is performed to evaluate the suitability of the model with actual conditions. Calculation of the χ^2 value in the Redlich-Peterson isotherm model for activated carbon SSAC and CAC obtained 0.0038 and 0.0094, where $\chi^2_{\text{count}} < \chi^2_{\text{table}}$. Therefore, there is no significant difference between the model and experimental results. The MSE and RMSE calculations show a very small value, and the model created has an insignificant error value.

3.9. Adsorption Kinetics. The kinetic process is the rate of change in the concentration of interacting materials. In a chemical reaction, the reaction rate demonstrates the velocity at which a reactant transforms into a product within a specified timeframe. However, in physical processes, such as adsorption, the interactions only involve the migration of a molecule or element from a less stable to a more stable region under the influence of van der Waals and electrostatic forces. van der Waals forces can explain the physical interaction between molecules or elements. In this study, the correlation of experimental data is analyzed with pseudo-

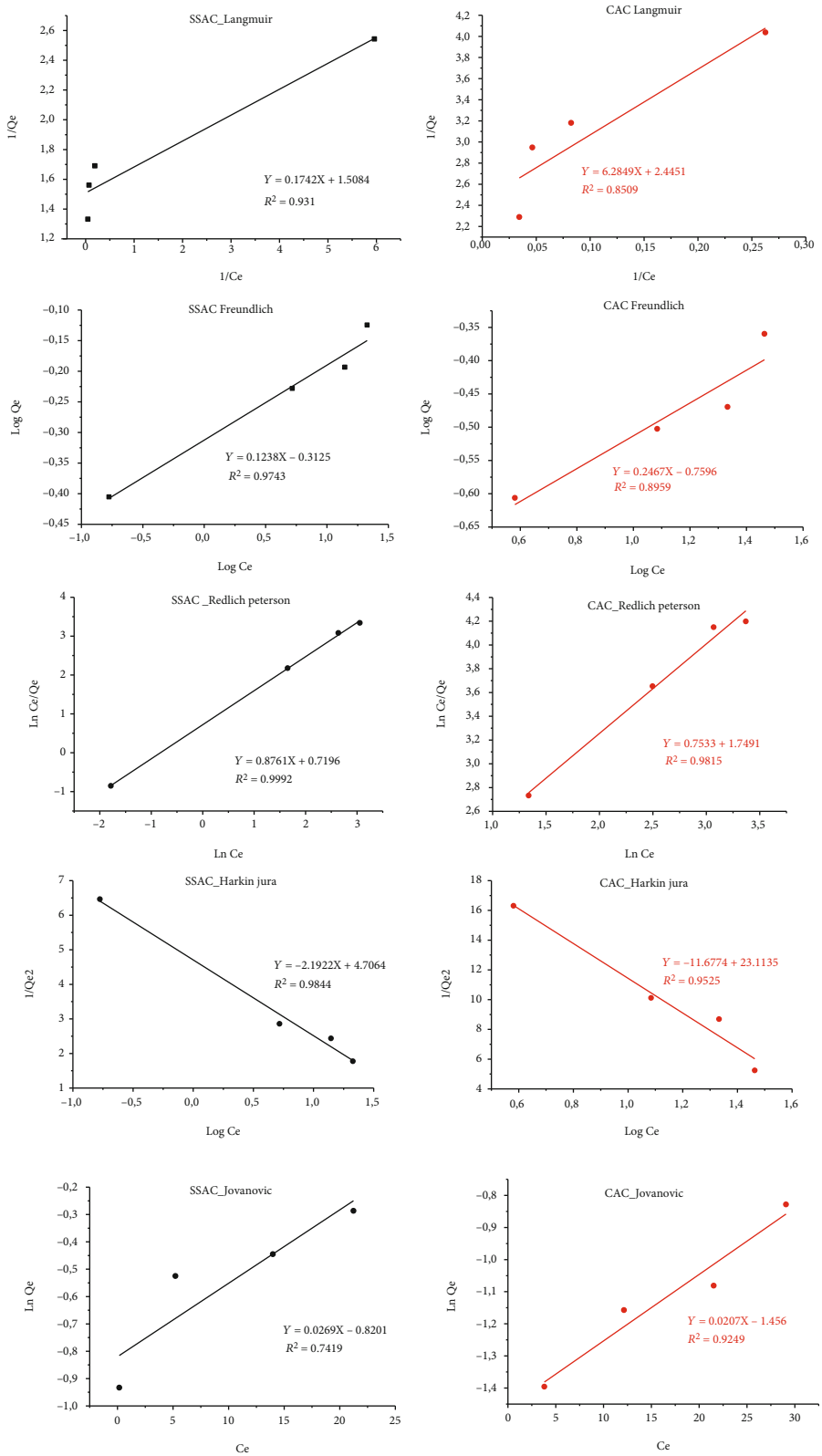

Figure 13: Adsorption isotherm modeling of copper ion with SSAC and CAC-activated carbon.

Table 3: Isoterm Langmuir and Freundlich in SSAC and CAC.

Isoterm	Parameters	SSAC	CAC
Langmuir	Q_m (mg/g)	0.663	0.409
	K_L (L/mg)	8.659	0.389
	R^2	0.931	0.8509
	R_L	0.003	0.0604
	χ^2	0.1169	0.029
	MSE	0.0145	0.0584
	RMSE	0.1204	0.2417
Freundlich	K_f (mg/g) $(L/mg)^{1/n}$	0.487	0.1739
	n	8.0775	4.0535
	R^2	0.9743	0.8959
	χ^2	0.0016	0.0005
	MSE	0.0003	0.0008
	RMSE	0.0165	0.0283
Redlich Peterson	A	2.0534	5.7495
	β	0.8761	0.7533
	R^2	0.9992	0.9815
	χ^2	0.00378	0.00935
	MSE	0.0015	0.0043
	RMSE	0.0382	0.0654
Harkin Jura	A	0.4562	0.0856
	B	2.1469	1.9793
	R^2	0.9844	0.9525
	χ^2	0.0699	1.0511
	MSE	0.0343	0.5070
	RMSE	0.1857	0.7121
Jovanovic	Q_{max} (mg/g)	0.4404	0.2322
	K_f (mg/g)	0.0269	0.0207
	R^2	0.7419	0.9249
	χ^2	0.0196	0.0041
	MSE	0.0098	0.0021
	RMSE	0.0989	0.0453

$\chi^2_{(1;0.05)} = 3.841$.

first-order, pseudo-second-order, Elovich, and Intraparticle diffusion adsorption kinetics models.

The pseudo-first-order equation is expressed as follows:

$$\frac{dQ_t}{dt} = k\,(Q_e - Q_t). \tag{9}$$

Integrating the equation concerning the given boundary conditions ($t = 0$, $Q_t = 0$ and $t = t$, $Q_e = Q_t$) yields the following formula [21]

$$\ln\,(Q_e - Q_t) = -k.t + \ln\,Q_e. \tag{10}$$

Which can be rearranged in a nonlinearized form [47]

$$Q_t = Q_e.\left(1 - e^{-k.t}\right). \tag{11}$$

From equation (6) (linear equation), the values of Q_e and Q_t are adsorption capacity at equilibrium and time t (mg/g), K_1 apparent pseudo-first-order rate constant (minutes $^{-1}$) adsorption process, and t is adsorption contact time (minutes). The values of Q_e and K_1 are obtained by plotting $\ln\,(Q_e - Q_t)$ versus t, with k_1 = slope and $\ln\,Q_e$ = intercept.

The pseudo-second-order equation can be expressed as follows [21]:

$$\frac{dQ_t}{dt} = \mathrm{k}.(Q_e - Q_t)^2. \tag{12}$$

Integrating the equation concerning the given boundary conditions ($t = 0$, $Q_t = 0$ and $t = t$, $Q_e = Q_t$) yields the following formula [21]:

$$Q_t = \frac{k_2.Q_e^2.t}{1 + k_2.Q_e.t}. \tag{13}$$

Then the equation above can be used as a basis for making a linear regression curve

$$\frac{t}{Q_t} = \frac{1}{Q_e}.t + \frac{1}{k_2.Q_e^2}. \tag{14}$$

The regression curve is plotted t/q_t and t as y-axis and x-axis. From the regression curve, the value $1/Q_e$ is obtained as $1/k_2.q_e^2$ to calculate K_2 value.

The Elovich rate equation is based on the adsorption capacity of an adsorbent and is used to depict the chemisorption kinetics of gases on heterogeneous solids. However, due to its limiting property of not capturing the slow kinetics of adsorption processes, the Elovich model is quite restricted in usage [21]. The Elovich model can be expressed as follows:

$$\frac{dQ_t}{dt} = \alpha_e\, e(-\beta_e Q_t), \tag{15}$$

where α is adsorption rate, β is the desorption constant, t is time, and K_t is a constant rate. After integrating the equation with the given conditions, $t = 0$, $Q_t = 0$ and $t = t$, $Q_t = Q_t$, the resulting equation is as follows:

$$Q_t = \frac{1}{\beta_e}\mathrm{Ln}(\alpha_e\beta_e) + \frac{1}{\beta_e}\mathrm{Lnt}. \tag{16}$$

Therefore, a linear plot of Q_t against $\mathrm{Ln}\,t$ can be made, with a slope of $1/\beta_e$ and an intercept of $(1/\beta_e)Ln\,(\alpha_e\beta_e)$.

The intraparticle diffusion model is used to understand the mechanism of diffusion involved in adsorption process [21]. Initially, the adsorbate molecules can migrate into the adsorbent surface from the bulk solution. These molecules further diffuse into the interior part of the adsorbent pore.

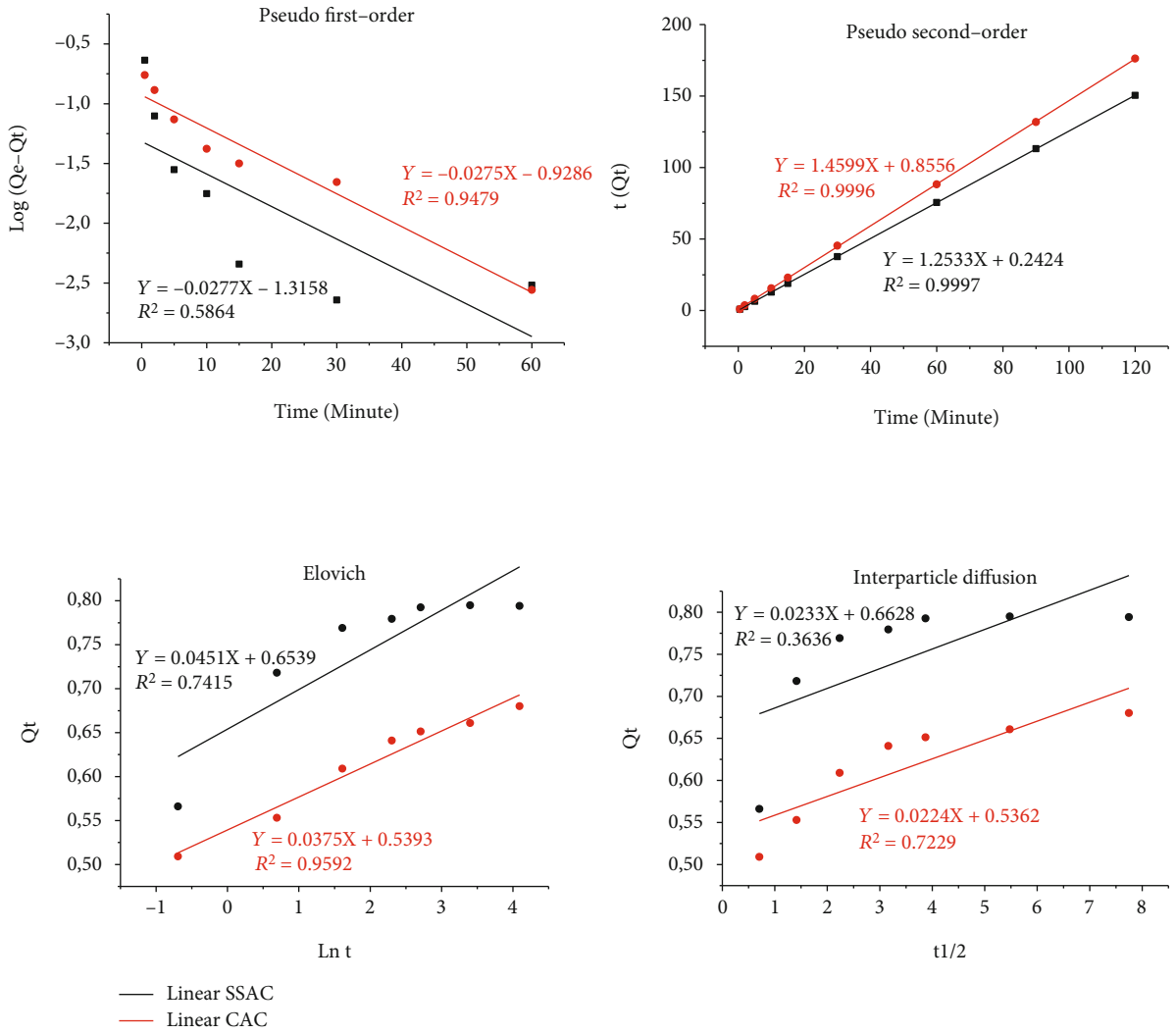

Figure 14: Linear graph of adsorption capacity over time and fitting curves of various models.

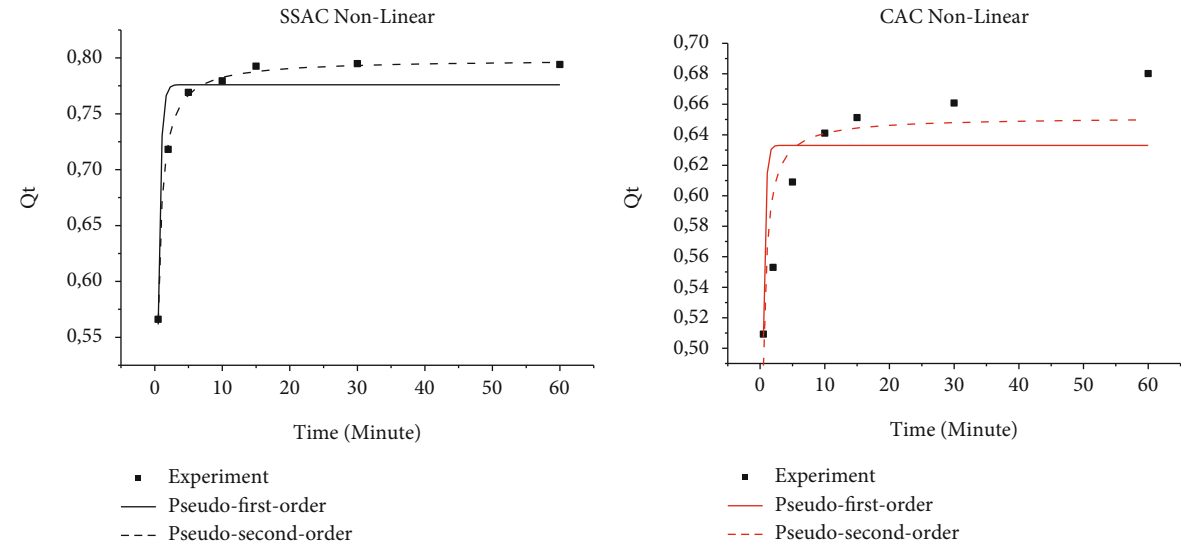

Figure 15: Nonlinear graph of adsorption capacity over time and fitting curve of various models.

Table 4: The summary of the calculation results.

Isoterm	Curve	Parameters	SSAC	CAC
Pseudo-first-order	Linear curve	K_{1L}	0.0633	0.0626
		R^2	0.5864	0.9479
		χ^2	1.5014	0.1193
		MSE	0.2023	0.0161
		RMSE	0.4497	0.1267
	Nonlinear curve	K_{1NL}	0.0588	0.0596
		R^2	0.8881	0.4763
		χ^2	0.0007	0.0020
		MSE	0.0005	0.0015
		RMSE	0.0235	0.0382
Pseudo-second-order	Linear curve	K_{2L}	6.48	2.49
		R^2	0.9997	0.9996
		χ^2	<0.0001	<0.0001
		MSE	0.0087	0.1956
		RMSE	0.0933	0.4423
	Nonlinear curve	K_{2NL}	6.23	2.24
		R^2	0.9978	0.7761
		χ^2	<0.0001	<0.0001
		MSE	0.00001	0.0006
		RMSE	0.0033	0.0249
Elovich	Linear curve	α	86.272	65.25
		R^2	0.7415	0.9592
		χ^2	0.0018	0.0002
		MSE	0.0013	0.0001
		RMSE	0.0358	0.0106
Interparticle diffusion	Linear curve	K_t	0.0233	0.0224
		R^2	0.7229	0.3657
		χ^2	0.0044	0.0011
		MSE	0.0032	0.0007
		RMSE	0.0562	0.0278

$\chi^2_{(1;0.05)} = 3.841$.

Adsorption takes place at the pore end of the adsorbent, while intraparticle diffusion occurs within the interior pores of the adsorbent [48]. The intraparticle diffusion model is given as follows:

$$Q_t = K_t t^{1/2} + C. \quad (17)$$

From equation (17), C is obtained as the intercept, and the intraparticle diffusion rate constant K_t (mg g.min$^{-0.5}$) is the slope from the linear plot of uptake (Q_t) versus the square root of time ($t^{1/2}$). The results of the regression curve equation are presented in Figure 14.

Determining the most appropriate adsorption kinetic model predictions is conducted by analyzing the (R^2) of each model. The correlation determination (R^2) shows the close relationship between points. Determining the model is performed by plotting the curve of simple linear and nonlinear equations. Adsorption kinetic model curve equation graph is shown in Figures 14 and 15 for linear and nonlinear curves. Subsequently, the summary of the calculation results is presented in Table 4.

The comparison between the four kinetic models of Cu^{2+} ion adsorption using SSAC- and CAC-activated carbon shows that the pseudo-second-order linear curve model exhibits the highest determination value. Specifically, the determination values are 0.9997 and 0.9996 for SSAC and CAC, respectively. In conclusion, adsorption kinetics of Cu^{2+} ions by activated carbon SSAC and CAC follow the pseudo-second-order linear model. The Chi-square (χ^2)

Table 5: Summarizes studies about copper removal using biomass material.

Biomass material	Processing/ activator	Optimum condition			Copper removal (%)	Adsorption capacity (mg/g)	Ref
		Contact time (minute)	pH	Adsorbent dose (g/l)			
Cellulose pulp waste	Water	180	6.00	20	80.00	1.55	[51]
Coconut shell	$ZnCl_2$	80	6.00	16	71.26	3.15	[52]
Minced banana peel	Water	20	3.00	2	90.00	0.33	[53]
Sugarcane bagasse	Citric acid	60	5.00	5	96.00	5.35	[54]
Sugarcane bagasse	NaOH	60	5.00	5	94.80	2.06	[54]
Samanea Saman	K_2CO_3	30	7.00	12.5	99.49	0.663	Present study

statistical test also reinforces this result, which gives the smallest result. In the Chi-square test, the smaller value χ^2_{count} indicates that the model compatibility with the experiment is improved. The calculation of error factor values, specifically MSE and RMSE, supports the observation that the utilized model exhibits minimal errors. These values indicate that the error of model is negligible and does not possess any significant deviation from the expected results.

The pseudo-second-order model is developed from metal adsorption experiments on solid materials. This is based on the assumption that divalent metal ions are adsorbed physical or chemical stage through sharing or exchanging electrons of metal ion compounds and the adsorbent. Therefore, adsorption capacity is proportional to the number of active sites on the surface of the adsorbent [49].

SSAC adsorption process speed is greater than CAC as seen from the value of the reaction rate constant in the linear graph equation, where K_{L2} SSAC is greater than K_{L2} CAC. The adsorption rate of the analyte is affected by the speed of the initial diffusion process of the particles on the surface of the adsorbent. The wider adsorbent surface allows the diffusion process to run faster and evenly. The graphical calculation of initial diffusion values for SSAC and CAC-activated carbon yields a value of 4.125 mg/g.minute and 1.168 mg/g.minute, respectively. Meanwhile, initial diffusion values are calculated from $1/k_2.q_e^2$ or 1/intercept linear graph [50].

A study on removing copper in solution has been carried out with various raw materials, activators, and other optimizations. In comparison to previous studies, activated carbon derived from SSAC demonstrates a notable improvement in the percentage of copper removal. The findings indicate that the optimum conditions encompass a shorter contact time, an optimal pH, and an increased efficiency in terms of the mass of adsorbent used. A comparison of the allowance percentage with previous studies is shown in Table 5. Using an environmentally friendly K_2CO_3 activator and carbonization-activation process can be an alternative for making activated carbon more energy efficient.

4. Conclusion

In conclusion, activated carbon derived from biomaterial through thermal and chemical activation processes was successfully investigated. Potassium carbonate (K_2CO_3) with a mass ratio (1 : 1) was used in the chemical activation of SSAC, and carbonization was carried out at 600°C for 5 h. Scanning electron microscopy and Fourier transform infrared spectroscopy results show a porous structure with different functions on the surface of SSAC. The authenticity of the study denoted that exploiting SS as a prominent but disregarded greening plant had been successfully performed. This was because adsorption performance of SSAC was better than CAC and adsorption isotherm was fitted with the Redlich-Peterson model. Furthermore, the kinetic modeling of copper adsorption on SSAC followed the pseudo-second-order. SS should be considered and proposed as a green alternative to commercial adsorbents for heavy metal wastewater. This study also highlighted the potential value of natural resource byproducts, such as SS, for the production of activated carbon. Other parameters, including temperature and reactor type, as well as the binary and ternary adsorption of tested pollutants, were examined for further investigation.

Data Availability

Data supporting available on request.

Conflicts of Interest

The authors declare that they have no conflicts of interest.

Acknowledgments

Funding research was supported by author team.

References

[1] N. Mabungela, N. D. Shooto, F. Mtunzi, and E. B. Naidoo, "The adsorption of copper, Lead metal ions, and methylene blue dye from aqueous solution by pure and treated fennel seeds," *Adsorption Science and Technology*, vol. 2022, article 5787690, pp. 1–21, 2022.

[2] ATSDR, "Copper | Toxic Substances | Toxic Substance Portal | ATSDR," 2019, https://wwwn.cdc.gov/TSP/substances/ToxSubstance.aspx?toxid=37 (accessed Oct. 31, 2022).

[3] J. Briffa, E. Sinagra, and R. Blundell, "Heavy metal pollution in the environment and their toxicological effects on humans," *Heliyon*, vol. 6, no. 9, article e04691, 2020.

[4] C. B. Godiya, X. Cheng, D. Li, Z. Chen, and X. Lu, "Carboxymethyl cellulose/polyacrylamide composite hydrogel for cascaded

treatment/reuse of heavy metal ions in wastewater," *Journal of Hazardous Materials*, vol. 364, pp. 28–38, 2019.

[5] L. Ezziat, A. Elabed, S. Ibnsouda, and S. el Abed, "Challenges of microbial fuel cell architecture on heavy metal recovery and removal from wastewater," *Frontiers in Energy Research*, vol. 7, p. 1, 2019.

[6] E. P. Kuncoro, T. Soedarti, T. W. C. Putranto, H. Darmokoesoemo, N. R. Abadi, and H. S. Kusuma, "Characterization of a mixture of algae waste-bentonite used as adsorbent for the removal of Pb2+ from aqueous solution," *Data in Brief*, vol. 16, pp. 908–913, 2018.

[7] N. Elboughdiri, "The use of natural zeolite to remove heavy metals Cu (II), Pb (II) and Cd (II), from industrial wastewater," *Cogent Engineering*, vol. 7, no. 1, 2020.

[8] C. Xu, S. Shi, X. Wang et al., "Electrospun SiO2-MgO hybrid fibers for heavy metal removal: characterization and adsorption study of Pb(II) and cu(II)," *Journal of Hazardous Materials*, vol. 381, article 120974, 2020.

[9] R. Katiyar, A. K. Patel, T.-B. Nguyen, R. R. Singhania, C.-W. Chen, and C.-D. Dong, "Adsorption of copper (II) in aqueous solution using biochars derived from *Ascophyllum nodosum* seaweed," *Bioresource Technology*, vol. 328, article 124829, 2021.

[10] S. Sangon, A. J. Hunt, T. M. Attard, P. Mengchang, Y. Ngernyen, and N. Supanchaiyamat, "Valorisation of waste rice straw for the production of highly effective carbon based adsorbents for dyes removal," *Journal of Cleaner Production*, vol. 172, pp. 1128–1139, 2018.

[11] Z. Deng, S. Sun, H. Li et al., "Modification of coconut shell-based activated carbon and purification of wastewater," *Advanced Composites and Hybrid Materials*, vol. 4, no. 1, pp. 65–73, 2021.

[12] L. Cundari, K. F. Sari, and L. Anggraini, "Characteristic of betel nuts activated carbon and its application to Jumputan wastewater treatment," *IOP Conference Series: Materials Science and Engineering*, vol. 345, no. 1, article 012041, 2018.

[13] A. C. Niam, E. Fenelon, E. Ningsih, Y. W. Mirzayanti, and E. Kristanti, "High-efficiency adsorption of hexavalent chromium from aqueous solution by *Samanea saman* activated carbon," *Adsorption Science and Technology*, vol. 2022, pp. 1–10, 2022.

[14] V. Sridevi, B. S. Rathi, P. S. Kumar et al., "Ultrasonic functionalized egg Shell powder for the adsorption of cationic dye: equilibrium and kinetic studies," *Adsorption Science and Technology*, vol. 2022, pp. 1–11, 2022.

[15] P. X. T. Nguyen, K. H. Ho, C. T. X. Nguyen et al., "Recent developments in water treatment by cellulose aerogels from agricultural waste," *IOP Conference Series: Earth and Environmental Science*, vol. 947, no. 1, article 012011, 2021.

[16] F. Ihsan and D. Rosleine, "Cooling effect to mitigate urban Heat Island by Pterocarpus indicus, Swietenia macrophylla and Samanea saman in Bandung, West Java Indonesia," *IOP Conference Series: Earth and Environmental Science*, vol. 528, no. 1, article 012057, 2020.

[17] R. K. Mishra, V. Kumar, and K. Mohanty, "Pyrolysis kinetics behaviour and thermal pyrolysis of *Samanea saman* seeds towards the production of renewable fuel," *Journal of the Energy Institute*, vol. 93, no. 3, pp. 1148–1162, 2020.

[18] H. N. Tran, S. J. You, and H. P. Chao, "Fast and efficient adsorption of methylene green 5 on activated carbon prepared from new chemical activation method," *Journal of Environmental Management*, vol. 188, pp. 322–336, 2017.

[19] A. H. Qusti, "Removal of chromium(VI) from aqueous solution using manganese oxide nanofibers," *Journal of Industrial and Engineering Chemistry*, vol. 20, no. 5, pp. 3394–3399, 2014.

[20] A. M. Aljeboree, A. N. Alshirifi, and A. F. Alkaim, "Kinetics and equilibrium study for the adsorption of textile dyes on coconut shell activated carbon," *Gazi University Journal of Science*, vol. 10, no. 4, pp. S3381–S3393, 2017.

[21] T. E. Amoo, K. O. Amoo, O. A. Adeeyo, and C. O. Ogidi, "Kinetics and equilibrium studies of the adsorption of copper(II) ions from industrial wastewater using activated carbons derived from sugarcane bagasse," *International Journal of Chemical Engineering*, vol. 2022, Article ID 6928568, 24 pages, 2022.

[22] H. N. Tran, H. P. Chao, and S. J. You, "Activated carbons from golden shower upon different chemical activation methods: synthesis and characterizations," *Adsorption Science and Technology*, vol. 36, no. 1–2, pp. 95–113, 2018.

[23] C. Saka, "BET, TG-DTG, FT-IR, SEM, iodine number analysis and preparation of activated carbon from acorn shell by chemical activation with $ZnCl_2$," *Journal of Analytical and Applied Pyrolysis*, vol. 95, pp. 21–24, 2012.

[24] O. Nurhilal, R. S. Lesmana, K. Ramadayanti et al., "Synthesis of high quality porous carbon from water hyacinth," *Key Engineering Materials*, vol. 860, pp. 173–177, 2020.

[25] M. Sánchez-Cantú, V. J. Janeiro-Coronel, J. A. Galicia-Aguilar, and J. D. Santamaría-Juárez, "Effect of the activation temperature over activated carbon production from castor cake and its evaluation as dye adsorbent," *International Journal of Environmental Science and Technology*, vol. 15, no. 7, pp. 1521–1530, 2018.

[26] H. Luo, W. Dou, and G. Li, "Study surface modified nanocellulose whiskers in coconut shell," *Journal of Physics Conference Series*, vol. 1948, no. 1, article 012190, 2021.

[27] C. A. Nunes and M. C. Guerreiro, "Estimation of surface area and pore volume of activated carbons by methylene blue and iodine numbers," *Quim Nova*, vol. 34, no. 3, pp. 472–476, 2011.

[28] A. I. Abd-Elhamid, E. A. Kamoun, A. A. El-Shanshory, H. M. A. Soliman, and H. F. Aly, "Evaluation of graphene oxide-activated carbon as effective composite adsorbent toward the removal of cationic dyes: composite preparation, characterization and adsorption parameters," *Journal of Molecular Liquids*, vol. 279, pp. 530–539, 2019.

[29] P. J. Wibawa, M. Nur, M. Asy'ari, and H. Nur, "SEM, XRD and FTIR analyses of both ultrasonic and heat generated activated carbon black microstructures," *Heliyon*, vol. 6, no. 3, article e03546, 2020.

[30] J. Hayat, M. Akodad, A. Moumen et al., "Phytochemical screening, polyphenols, flavonoids and tannin content, antioxidant activities and FTIR characterization of *Marrubium vulgare* L. from 2 different localities of Northeast of Morocco," *Heliyon*, vol. 6, no. 11, article e05609, 2020.

[31] M. Zahoor, M. Wahab, S. M. Salman, A. Sohail, E. A. Ali, and R. Ullah, "Removal of Doxycycline from Water using *Dalbergia sissoo* Waste Biomass Based Activated Carbon and Magnetic Oxide/Activated Bioinorganic Nanocomposite in Batch Adsorption and Adsorption/Membrane Hybrid Processes," *Bioinorganic Chemistry and Applications*, vol. 2022, Article ID 2694487, 17 pages, 2022.

[32] R. Han, W. Zou, Y. Wang, and L. Zhu, "Removal of uranium(VI) from aqueous solutions by manganese oxide coated

zeolite: discussion of adsorption isotherms and pH effect," *Journal of Environmental Radioactivity*, vol. 93, no. 3, pp. 127–143, 2007.

[33] M. Kavand, P. Eslami, and L. Razeh, "The adsorption of cadmium and lead ions from the synthesis wastewater with the activated carbon: optimization of the single and binary systems," *Journal of Water Process Engineering*, vol. 34, article 101151, 2020.

[34] A. Temesgen Abeto, S. M. Beyan, B. Abreham Bekele, and K. Worku Firomsa, "Optimization and modeling of Cr (VI) removal from tannery wastewater onto activated carbon prepared from coffee husk and sulfuric acid (H2SO4) as activating agent by using central composite design (CCD)," *Journal of Environmental and Public Health*, vol. 2023, Article ID 5663261, 14 pages, 2023.

[35] E. Demirbas, N. Dizge, M. T. Sulak, and M. Kobya, "Adsorption kinetics and equilibrium of copper from aqueous solutions using hazelnut shell activated carbon," *Chemical Engineering Journal*, vol. 148, no. 2–3, pp. 480–487, 2009.

[36] S. H. Dewi and D. Ridwan, "Sintesis dan Karakterisasi Nanopartikel Fe3O4 Magnetik Untuk Adsorpsi Kromium Heksavalen," *Jurnal Sains Materi Indonesia Indonesian Journal of Materials Science*, vol. 13, no. 2, p. 1411, 2012.

[37] Y. A. B. Neolaka, Y. Lawa, J. Naat et al., "Efficiency of activated natural zeolite-based magnetic composite (ANZ- Fe_3O_4) as a novel adsorbent for removal of Cr(VI) from wastewater," *Journal of Materials Research and Technology*, vol. 18, pp. 2896–2909, 2022.

[38] R. Nadeem, M. A. Naqvi, M. H. Nasir et al., "Efficacy of physically pretreated *Mangifera indica* biomass for Cu^{2+} and Zn^{2+} sequestration," *Journal of Saudi Chemical Society*, vol. 19, no. 1, pp. 23–35, 2015.

[39] A. A. Alghamdi, A. B. Al-Odayni, W. S. Saeed, A. Al-Kahtani, F. A. Alharthi, and T. Aouak, "Efficient Adsorption of Lead (II) from Aqueous Phase Solutions Using Polypyrrole-Based Activated Carbon," *Materials*, vol. 12, p. 2020, 2019.

[40] A. Nasrullah, A. S. Khan, A. H. Bhat et al., "Effect of short time ball milling on physicochemical and adsorption performance of activated carbon prepared from mangosteen peel waste," *Renewable Energy*, vol. 168, pp. 723–733, 2021.

[41] M. A. Al-Ghouti and D. A. Da'ana, "Guidelines for the use and interpretation of adsorption isotherm models: a review," *Journal of Hazardous Materials*, vol. 393, article 122383, 2020.

[42] E. Siswoyo, Y. Mihara, and S. Tanaka, "Determination of key components and adsorption capacity of a low cost adsorbent based on sludge of drinking water treatment plant to adsorb cadmium ion in water," *Applied Clay Science*, vol. 97-98, pp. 146–152, 2014.

[43] H. Chen, J. Zhao, G. Dai, J. Wu, and H. Yan, "Adsorption characteristics of Pb(II) from aqueous solution onto a natural biosorbent, fallen *Cinnamomum camphora* leaves," *Desalination*, vol. 262, no. 1–3, pp. 174–182, 2010.

[44] N. Ayawei, A. N. Ebelegi, and D. Wankasi, "Modelling and interpretation of adsorption isotherms," *Journal of Chemistry*, vol. 2017, Article ID 3039817, 11 pages, 2017.

[45] F. Brouers and T. J. Al-Musawi, "On the optimal use of isotherm models for the characterization of biosorption of lead onto algae," *Journal of Molecular Liquids*, vol. 212, pp. 46–51, 2015.

[46] R. Ragadhita and A. B. D. Nandiyanto, "How to calculate adsorption isotherms of particles using two-parameter monolayer adsorption models and equations," *Indonesian Journal of Science and Technology*, vol. 6, no. 1, pp. 205–234, 2021.

[47] H. Moussout, H. Ahlafi, M. Aazza, and H. Maghat, "Critical of linear and nonlinear equations of pseudo-first order and pseudo- second order kinetic models," *Karbala International Journal of Modern Science*, vol. 4, no. 2, pp. 244–254, 2018.

[48] G. Bharath Balji and P. Senthil Kumar, "Adsorptive removal of alizarin red S onto sulfuric acid-modified avocado seeds: kinetics, equilibrium, and thermodynamic studies," *Adsorption Science and Technology*, vol. 2022, article 3137870, pp. 1–13, 2022.

[49] Y. S. Ho and G. McKay, "Pseudo-second order model for sorption processes," *Process Biochemistry*, vol. 34, no. 5, pp. 451–465, 1999.

[50] G. Sharma, S. Sharma, A. Kumar et al., "Activated carbon as Superadsorbent and sustainable material for diverse applications," *Adsorption Science and Technology*, vol. 2022, article 4184809, pp. 1–21, 2022.

[51] M. Ulmanu, E. Marañón, Y. Fernández, L. Castrillón, I. Anger, and D. Dumitriu, "Removal of copper and cadmium ions from diluted aqueous solutions by low cost and waste material adsorbents," *Water, Air, and Soil Pollution*, vol. 142, no. 1/4, pp. 357–373, 2003.

[52] E. Bernard, A. Jimoh, and J. O. Odigure, "Heavy Metals Removal from Industrial Wastewater by Activated Carbon Prepared from Coconut Shell," *Research Journal of Chemical Sciences*, vol. 3, no. 8, pp. 3–9, 2013, Jan. 21, 2023. http://www.isca.in.

[53] R. S. D. Castro, L. Caetano, G. Ferreira et al., "Banana Peel applied to the solid phase extraction of copper and Lead from river water: Preconcentration of metal ions with a fruit waste," *Industrial and Engineering Chemistry Research*, vol. 50, no. 6, pp. 3446–3451, 2011.

[54] M. Gupta, H. Gupta, and D. S. Kharat, "Adsorption of cu(II) by low cost adsorbents and the cost analysis," *Environmental Technology and Innovation*, vol. 10, pp. 91–101, 2018.